PROBABILITY FUNCTIONALS, HOMOGENIZATION AND COMPREHENSIVE RESERVOIR SIMULATORS

K. TUNCAY* AND P. ORTOLEVA[†]

Abstract. A probability functional method is used to determine the most probable state of a reservoir or other subsurface features. The method is generalized to arrive at a self-consistent accounting of the multiple spatial scales involved by unifying information and homogenization theories. It is known that to take full advantage of the approach (e.g. to predict the spatial distribution of permeability, porosity, multiphase flow parameters, stress, fracturing) one must embed multiple reaction, transport, mechanical (RTM) process simulators in the computation. A numerical technique is introduced to directly solve the inverse problem for the most probable distribution of reservoir state variables. The method is applied to several two and three dimensional reservoir delineation problems.

1. Introduction. The state of a reservoir or other subsurface feature is generally only known at selected space-time points on a rather coarse scale. Yet we would like to reconstruct the spatial distribution of fluid/rock state across a reservoir or other system. As we would like to determine such fluid/rock variables as functions of position and as the subsurface can only be determined with great uncertainty, we must use a probability functional formalism - i.e. analyze the probability of a continuous infinity of variables needed to describe the distribution of properties across the system.

This goal cannot be accomplished without the use of models that describe many fluid/rock variables. For example, a classical history matching procedure using a single phase flow model could not be used to determine the preproduction oil saturation across a system. As a complete understanding of reservoir state involves the fluid saturations, nature of the wetting, porosity, grain size and mineralogy, stress, fracture network statistics, etc., it is clear that hydrologic simulators are needed that account for a full suite of reaction, transport, and mechanical (RTM) processes. It is thus the goal of this communication to present our probability functional – RTM reservoir simulator approach to the complete characterization of a subsurface system.

We expect that the state of a reservoir involves variations in space over a wider range of length scales. As suggested in Fig. 1, the shape and internal characteristics of a reservoir can vary on a wide range of scales including those shorter than the scale on which the observations could resolve. For example, knowing fluid pressure at wells separated by 1 km could not uniquely determine variations of permeability on the 10 cm scale. Therefore one most consider the determination of the most probable state

---

*Department of Geochemistry, Faculty of Earth Sciences, Utrecht University, P.O. Box 80021, 3508 TA Utrecht, The Netherlands.

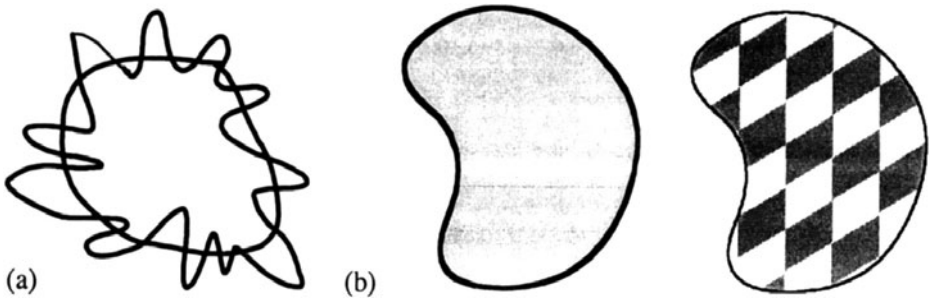†Laboratory for Computational Geodynamics, Department of Chemistry, Indiana University, Bloomington, IN 47405.

FIG. 1. *(a) Both smooth and short-scale profiles for the demarcation of a super-K (anomalously high permeability) zone, compartment or reservoir. Such complexity can even be fractal in nature and still be consistent with available data. The region of uniform permeability. (b) is not distinguishable from a mosaic of low (white) and high (dark) regions. (c) when only data of coarse spatial resolution is known.*

among the unrestricted class of states that can involve variations on all spatial scales. In Fig. 2 we suggest that the probability ρ_k of variations on a length scale $2\pi/k$ must become independent of k as $k \to \infty$. Thus in a classic history matching approach there is an uncountable infinity of solutions. In our approach we seek the most probable upscaled state consistent with the scale on which the observations are taken.

Geostatistical methods are extensively used to construct the state of a reservoir. Traditional geostatistical methods utilizes the static data from core characterizations, well logs, seismic or similar types of information. However, since the relation between production and monitoring well data (and other type of dynamic data) and reservoir state variables is quite complicated, traditional geostatistical approaches fail to integrate dynamic and static data. Two significant methods have been developed to integrate the dynamic flow of information from production and monitoring wells, and the static data. The goal of both methods is to minimize an "objective function" that is constructed to be a measure of error between observations and predictions. The multiple data sets are taken into consideration by introducing weighting factors for each data set. The first method (sequential self-calibration) defines a number of master points (which is less than the number of grid points on which the state of the reservoir is to be computed). Then a reservoir simulation is performed for an initial guess of the
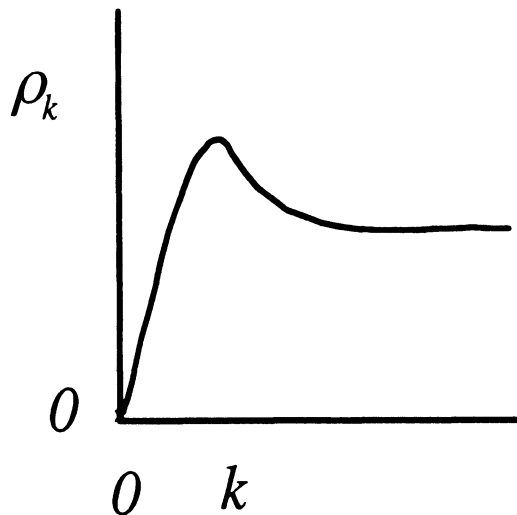
FIG. 2. *The probability for variations of wave vector k must become independent of k for large k as the sparceness of the data does not allow one to discriminate among all the short scale (large k) states.*

reservoir state variables that is obtained by the use of traditional geostatistical methods. The nonlinear equations resulting from the minimization of the objective function requires the calculation of derivatives (sensitivity coefficients) with respect to the reservoir state variables. The approximate derivatives are efficiently obtained by assuming that streamlines do not change because of the assumed small perturbations in the reservoir state variables. In summary, the sequential self-calibration method first upscales the reservoir using a multiple grid-type method and then uses stream line simulators to efficiently calculate the sensitivity coefficients. A difficulty in this procedure is that convergence to an acceptable answer is typically not monotonic (and is thereby slow and convergence is difficult to assess). The second method (gradual deformation) expresses the reservoir state as a weighted linear sum of the reservoir state at the previous iteration and two new independent states. The three weighting factors are determined by minimizing the objective function. The procedure is iterated using a Monte Carlo approach to generate new states. Comparisons of the two methods are presented in Wen et al. (1997,2000). Sequential self-calibration is discussed by Gomez-Hernandez et al. (1998), Wen et al. (1998a,b 1999), and Tran et al. (1999) whereas gradual deformation is discussed in Roggero and Hu (1998), Hu et al. (1999), and Hu (1999).

  2. Probability functional approach. Let a reservoir be characterized by a set of variables $\Psi(\vec{r})$ at all points $\vec{r}$ within the system at a given time. For example, $\Psi(\vec{r})$ may represent the values of porosity, grain size

and mineralogy, stress, fractures, petroleum vs. water saturation and state of wetting before production began. We seek the probability $\rho[\Psi]$ that is a functional of Ψ and, in particular, wish to construct it to be consistent with a set of observations $O(= \{O_1, O_2, \ldots O_N\})$ at various points across the system or at various times. In addition, we assume that we have an RTM reservoir simulator that can compute these observables given an initial state $\Psi(\vec{r})$. We let $\Omega(= \{\Omega_1, \Omega_2, \ldots \Omega_N\})$ be the set of computed values corresponding to O. Clearly, Ω is a functional of $\Psi(\vec{r})$.

Information theory provides a prescription for computing probability. For the present problem, the prescription may be stated as follows. The entropy S is defined via

$$(2.1) \qquad\qquad S = -\mathop{\mathbf{S}}_{\Psi} \rho \ell n \rho$$

where $\mathbf{S}$ indicates a functional integral. Normalization implies

$$(2.2) \qquad\qquad \mathop{\mathbf{S}}_{\Psi} \rho = 1.$$

The entropy is to be maximized subject to a set of constraints from the known information. Let $C(= \{C_1, C_2, \ldots C_{N_c}\})$ be a set of constraints that depend on O and Ω and, therefore, are functionals of Ψ. We introduce two types of constraints. One group, the "error constraints," are constructed to increase monotonically with the discrepancy between O and Ω. A second group places bounds on the spatial resolution (the length scale) over which we seek to delineate the reservoir attributes. These constraints are required for self-consistency as the reservoir simulators typically used assume a degree of upscaling imposed by a lack of short scale information and practical limits to CPU time. In all cases the constraints are functionals of $\Psi(C = C[\Psi])$ and we impose the "information"

$$(2.3) \qquad\qquad \mathop{\mathbf{S}}_{\Psi} \rho C_i = \Gamma_i, \quad i = 1, 2, \ldots N_c.$$

Using the Lagrange multiplier method we obtain maximum entropy consistent with (2.2), (2.3) in the form

$$(2.4) \qquad\qquad \ell n \rho = -\ell n \Xi - \sum_{i=1}^{N_c} \beta_i C_i[\Psi]$$

$$(2.5) \qquad\qquad \Xi = \mathop{\mathbf{S}}_{\Psi} \exp\left[\sum_{i=1}^{N_c} \beta_i C_i\right].$$

The β's are Lagrange multipliers and is the normalization constant.

In our approach we focus on the most probable state Ψ^m. The maximum in occurs when

$$(2.6) \qquad\qquad \sum_{i=1}^{N_c} \beta_i \frac{\delta C_i}{\delta \Psi_\alpha(\vec{r})} = 0.$$

Here $\delta/\delta\Psi_\alpha$ indicates a functional derivative with respect to the $\alpha - th$ fluid/rock state variable. We solve these functional differential equations for the spatial distribution of the N reservoir attributes $\Psi_1^m(\vec{r}), \Psi_2^m(\vec{r}), \dots$ $\Psi_N^m(\vec{r})$.

There are two sets of conditions necessary for the solution of (2.5). The character of the homogenization constraints is that they only have an appreciable contribution when Ψ has spatial variations on a length scale smaller than that assumed to have been averaged out in the upscaling underlying the RTM reservoir models used to construct the Ψ-dependence of the Ω.

3. Comprehensive RTM reservoir models. The functional dependence of the predicted values $\Omega[\Psi]$ on the spatial distribution of reservoir state $\Psi(\vec{r})$ is determined by the laws of physics and chemistry that evolve the "fundamental" fluid/rock state variables Ψ. We consider these fundamental variables to include (see Ortoleva 1994a,b, 1998; Tuncay and Ortoleva 2001, Tuncay, Park and Ortoleva 2000a,b; Ozkan and Ortoleva 2000)

- stress;
- fluid composition, phases and their intra-pore scale configuration (e.g. wetting, droplet or supra-pore scale continuous phase);
- grain size, shape, packing, and mineralogy and their statistical distribution;
- fracture network statistics; and
- temperature.

With these variables we can predict the derivative quantities (e.g. phenomenological parameters for the RTM process laws).

- permeability;
- relative permeabilities, capillary pressure and other multi-phase parameters;
- rock rheological parameters; and
- thermal conductivity.

From the latter one you can, through the solution of reservoir RTM equations, determine the functionals $\Omega[\Psi]$. Thus we consider Ψ to be the set of fundamental variables at some reference time (e.g. just prior to petroleum production or pollutant migration). The dependence of Ω on Ψ comes from the solution of RTM equations and the use of phenomenological laws relating the derived quantities to the fundamental ones.

A complex network of geochemical reactions, fluid and energy transport and rock mechanical (RTM) processes underlies the genesis, dynamics and characteristics of petroleum reservoirs and other subsurface features (Ortoleva et al. 1997; Ortoleva 1998; Tuncay, Park and Ortoleva 2000a,b; Tuncay and Ortoleva 2001). Prediction of reservoir location and producibility lies outside the realm of simple approaches. In order to develop a predictive capability for reservoir location and characteristics, we have developed

the quantitative basin/reservoir simulator, Basin RTM. This simulator integrates all the relevant geological factors and RTM processes. As reservoirs are fundamentally 3-D in nature, Basin RTM was developed in terms of a fully 3-D finite element approach. The specific process and rate laws used in Basin RTM are reviewed in Ortoleva (1994a,b, 1998), Ortoleva et. al (1997), Payne et al (2000), and Tuncay Park and Ortoleva (2000a,b).

The following features show the comprehensiveness of our rock/fluid state description and the completeness of the set of chemical and physical processes evolving them.

• Incremental stress rheology (Zienkiewicz and Cormeau 1974; Rice 1975) is used to integrate poroelasticity, viscous flow with yield behavior, fracturing and pressure solution. In most studies sediments are considered as either nonlinear Newtonian fluids or as elastic media, thereby ignoring the effects of faulting and fracturing (Ortoleva 1994a, 1998; Tuncay, Park and Ortoleva 2000a,b; Ortoleva et al. 1997).

• Faulting occurs via a Drüker-Prager criterion to signal failure, and a texture dynamics model is used to compute the evolving, associated rheologic properties (Tuncay, Khalil and Ortoleva 2001).

• Petroleum generation/rock deformation and multi-phase flow are solved simultaneously to capture seals, abnormally pressured compartments and petroleum expulsion.

• Inorganic and organic solid state and fluid reactions and their temperature and ionic state dependencies are accounted for (Ortoleva 1994a,b, 1998).

• Grain growth/dissolution, breaking of grain-grain contacts, pressure solution and gouge evolve rock texture (Ortoleva 1994a,b, 1998, Ozkan and Ortoleva 2000).

• A 3-D fracture network dynamics has been developed that accounts for the stress tensor, fluid pressure and rock texture variables (Fig. 3) (Tuncay, Park and Ortoleva 2000a,b).

• A 3-D computational platform is used. All other basin simulators are limited to 2-D or a few processes. Nonlinear dynamical systems have a strong dependence on spatial dimensionality (Ortoleva et al. 1987a,b; Ortoleva 1990, 1992, 1994a,b). Therefore, a 3-D computational platform is required to gain a better understanding of fracture networks and reservoirs and the dynamical petroleum system (Figs. 4).

The processes and phenomenological laws embedded in Basin RTM are now being used to develop a next-generation class of 3-D multiple RTM process reservoir simulators to capture reservoir evolution on the engineering time scale. We thus are able to use the information theory approach of the previous section to determine a variety of fluid/rock properties in the preproduction state as they vary across a reservoir or subsurface pollution site.
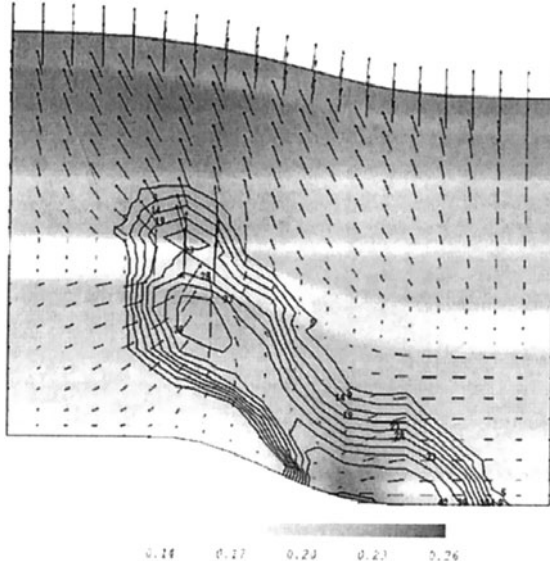
FIG. 3. *Cross-section of a 2-D, 5×2.5 km normal fault system after 5 My of simulation. The shading indicates porosity and shows differences between the four lithologies; the shales (low porosity) are at the middle and top of the domain. Higher porosity regions (in the lower-right and upper-left corners) and the fracture length (contour lines) arose due to the deformation created by differential subsidence. Both stress field and fracturing are strongly affected by rock composition and texture. The arrows indicate fluid flow toward the region of increasing porosity (lower-right) and through the most extensively fractured shale.*

4. Homogenization.

Homogenization theory provides a prescription for computing the effective transport and other properties for upscaled computation. Here we investigate its use in formulating the two scale permeability problem to yield a self-consistent procedure for computing the most probable distribution of homogenized permeability. We illustrate our procedure for the case of steady single phase Darcy flow.

The starting point of our analysis is the assumption that the permeability K has a long spatial scale dependence and a short scale dependence $\vec{r}_0$ related by $\vec{r}_1 = \varepsilon \vec{r}_0$ for $\varepsilon \leq 1$. We modify this traditional view somewhat and conceive of space $\vec{r}_1$ as having an associated set of permeability variables $K(\vec{r}_0, \vec{r}_1)$ — the distribution of the values of K in a small region about $\vec{r}_1$. In this small region (representative volume) $K(\vec{r}_0, \vec{r}_1)$ varies periodically or has a statistically representative set of variations for K near $\vec{r}_1$.

Fig. 5 is a schematic depiction of a discretized form of our two scale concept. There is a macrogrid (with elements centered at points $\vec{r}_1$) and with each macronode there is a set of micronodes centered about points $\vec{r}_0$.

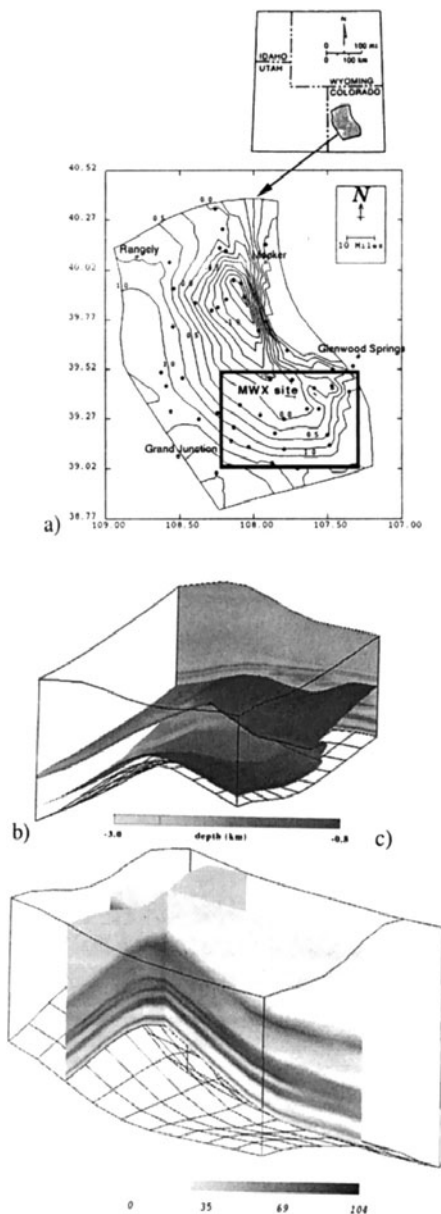Using multiple scale analysis, the steady state pressure P is expanded in the form

FIG. 4. a) Simulation domains for basin-scale and inter-field studies (thickly outlined box). The Rulison Field is in the upper northwestern area of the latter box. b) Isosurface of overpressure (15 bars) toned with depth. The folded, multi-layered structure is dictated by the interplay of lithological differences and fracturing and shows the three-dimensional complexity of conductivity of overpressured zones. Thus, stacked overpressured compartments as viewed as a simple pressure-depth curve may hold little insight into the full three-dimensionality of the structure. c) The distribution of fracture length reflects lithologic variation and the topography imposed by the basement tectonics. The layered fracture length structure is closely related to the layering in overpressure surface.
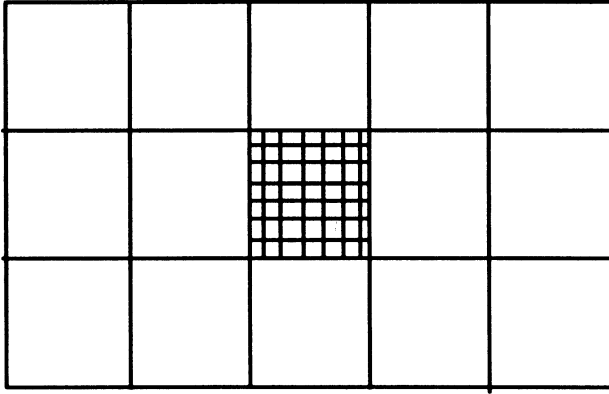
FIG. 5. *Macrogrid discretizing $\vec{r}_1$ space with embedded microgrid descretizing $\vec{r}_0$ space.*

(4.1) $$P = P_0(\vec{r}_1) + \varepsilon P_1(\vec{r}_0, \vec{r}_1) + \cdots .$$

With this the pressure error E can be written in terms of the pressure P_i^{obs} at each of the N_{obs} observation wells $(i = 1, 2, \ldots N_{obs})$:

(4.2) $$E = \sum_{i=1}^{N_{obs}} (P_{0i} + \varepsilon P_{1i} + \cdots - P_i^{ob})^2$$

where P_i^{ob} is the pressure at monitoring site i. Thus

(4.3) $$E = E_0[K^h] + 2\varepsilon \sum_{i=1}^{N_{obs}} (P_{0i} - P_i^{obs}) P_{1i},$$

where E_0 is the error as computed using an upscaled reservoir simulator with permeability K^h. Collecting powers of ε in the equation of steady Darcy flow one obtains the hierarchy

(4.4) $$\vec{\nabla}_0 \cdot (K \vec{\nabla}_0 P_1) + \vec{\nabla}_0 K \cdot \vec{\nabla}_1 P_0 = 0$$

(4.5) $$\vec{\nabla}_0 \cdot (K \vec{\nabla}_0 P_2) + \vec{\nabla}_1 \cdot (K \vec{\nabla}_0 P_1) + \vec{\nabla}_0 \cdot (K \vec{\nabla}_1 P_1) + \vec{\nabla}_1 \cdot (K \vec{\nabla}_1 P_0) = 0$$

Equation (4.4) implies

(4.6) $$P_1 = \sum_{\alpha=1}^{3} G_\alpha \frac{\partial P_0}{\partial x_{1\alpha}}$$

where the G_α are the solutions of

(4.7) $$\vec{\nabla}_0 \cdot (K \vec{\nabla}_0 G_\alpha) + \frac{\partial K}{\partial x_{0\alpha}} = 0.$$

With this we obtain

$$(4.8) \quad E = E[K^h] + 2\varepsilon \sum_{i=1}^{N_0}(P_{0i} - P_i^{obs}) \sum_{\alpha=1}^{3} G_\alpha[K]\left(\frac{\partial P_0}{\partial x_{1\alpha}}\right)_i + O(\varepsilon^2).$$

Averaging (4.4) over one realization of a representative volume one obtains

$$(4.9) \quad \sum_{\alpha_1,\alpha_2=1}^{3} \frac{\partial}{\partial x_{1\alpha_1}}\left(K^h_{\alpha_1\alpha_2}\frac{\partial P_0}{\partial x_{1\alpha_2}}\right) = 0$$

$$(4.10) \quad K^h_{\alpha_1\alpha_2} = \frac{1}{V^{rep}}\int_{V^{rep}} d^3r_0 K\left[\delta_{\alpha_1\alpha_2} + \frac{\partial G_{\alpha_2}}{\partial x_{0\alpha_1}}\right].$$

The probability ρ as in Section 2 is a functional of K and, in the discretized form as suggested in Fig. 5, ρ is a function of $K(\vec{r}_0, \vec{r}_1)$. Note that K^h is a complex function of K.

To construct the probability we impose the condition

$$(4.11) \quad \underset{K}{\mathbf{S}}\rho E = E^*$$

noting that this implies a functional integral over all K, i.e. all possible $\vec{r}_0$ and $\vec{r}_1$ dependencies. We impose two conditions on the maximization of the entropy so as to characterize the likely scales on which the permeability can fluctuate:

$$(4.12) \quad \underset{K}{\mathbf{S}}\rho \int d^6r \left|\vec{\nabla}_1 K\right|^2 = A_1$$

$$(4.13) \quad \underset{K}{\mathbf{S}}\rho \int d^6r \left|\vec{\nabla}_0 K\right|^2 = A_2$$

where $d^6r = d^3r_0 d^3r_1$. This implies that takes the form

$$(4.14) \quad \ell n\rho = -\ell n\Xi - \beta_0 E - \beta_1 \int d^6r \left|\vec{\nabla}_1 K\right|^2 - \beta_2 \int d^6r \left|\vec{\nabla}_0 K\right|^2.$$

The β_1, β_2 terms fix the minimal spatial scales over which $\vec{r}_0$ and $\vec{r}_1$ are like to vary.
Finally,

$$(4.15) \quad \Xi = \underset{K}{\mathbf{S}}\exp\left\{-\beta_0 E - \beta_1 \int d^6r_1 \left|\vec{\nabla}_1 K\right|^2 - \beta_2 \int d^6r_0 \left|\vec{\nabla}_0 K\right|^2\right\}.$$

With this, the most probable distribution satisfies

$$(4.16) \quad \frac{\delta E}{\delta K} - \lambda_1 \Delta_1^2 K - \lambda_2 \Delta_0^2 K = 0$$
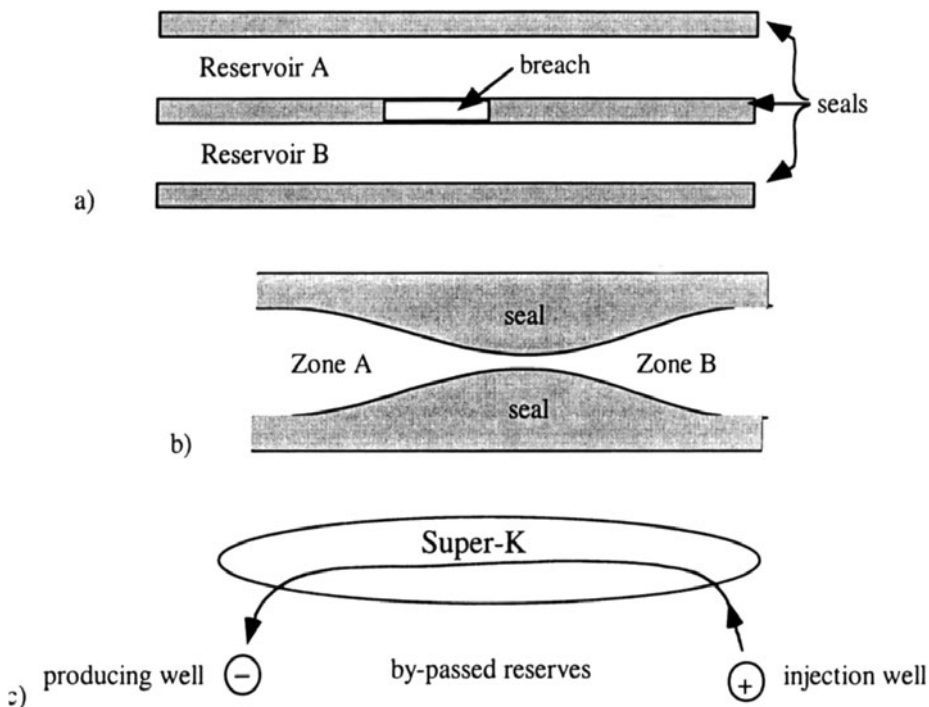
FIG. 6. *Schematic view of systems plagued with heterogeneity that can lead to by-passed reservoirs. In case (a) the upper and lower reservoirs are separated by a seal which is compromised in some poorly defined region. (b) Pinchout separates a sandstone reservoir into two poorly connected regimes. c) A zone of super-K can direct flows around petroleum-saturated matrix and thus lead to by-passing of reserves.*

where $\lambda_1 = 2\beta_1/\beta_0$ and similarly for λ_2. Averaging over a representative volume V^{rep} of $\vec{r}_0$-space and using the expression for E to order ε yields

$$(4.17) \quad \frac{\delta E_0}{\delta K^h}\left\langle \frac{\delta K^h}{\delta K} \right\rangle + 2\varepsilon \sum_{i=1}^{N_0}(P_{0i} - P^{obs}) \sum_{\alpha=1}^{3} \frac{\partial P_0}{\partial x_{1\alpha}}\langle G_\alpha \rangle - \lambda_1 \Delta_1^2 \langle K \rangle = 0$$

where $\langle \ldots \rangle$ is an average of a quantity over a representative volume about $\vec{r}_1$. Note that

$$(4.18) \qquad K_{\alpha_1,\alpha_2}^h = \langle K \rangle \delta_{\alpha_1\alpha_2} + \left\langle K \frac{\partial G_{\alpha_1}}{\partial x_{0\alpha_2}} \right\rangle.$$

To make the evaluations of interest we must compute the three G_α.

5. Numerical simulations. In the cases shown in Fig. 6, there are difficulties in placing wells and planning the best production rates from existing wells to minimize by-passed reserves and excessive water cuts. The

key to making successful decisions is quantifying the geometry of reservoir connectivity or compartmentation. Our technology places quantitative limits on the location, shape and extent of the zones of super-K or connectivity to other reservoirs or parts of the same, multi-lobed reservoir.

Information theory is used in our approach to provide a mathematical framework for assessing risk. We use the information theory software to integrate quantitative reservoir simulators with the available field data. Our approach allows one to:

- use field data of various types and quality;
- integrate the latest advances in reservoir or basin modeling/ simulation into production planning and reserve assessment;
- predict the quantitative state (distribution of porosity, permeability, stress, reserves in place) across the system;
- place quantitative bounds on all uncertainties involved in our predictions/strategies; and
- carry out all the above in one automated procedure.

This technology will improve the industry's ability to develop known fields and identify new ones by use of all the available seismic, well log, production history, and other observations.

Fig. 7 shows a 2-D test case domain (10×10 km). The pressure monitoring wells are shown with dots in Fig. 7a. In this example, we demonstrate our multiple gridding approach. We first obtain a coarse permeability field and then use it as our initial guess for a finer resolved permeability field. This process reduces the computational effort to arrive at the most probable permeability field since it takes only a few iterations to solve the coarsely resolved problem. Fig. 8 shows another 2-D example where only two permeability logs are available. Although both permeability logs miss the puncture in the center, our approach results in lower permeability at both ends of the domain and higher permeability in the center. This example demonstrates that the core and well log data can be directly imposed in the most probable reservoir state in our approach, making our approach cost effective. As seen in Fig. 9, our approach can also successfully predict the initial pressure distribution showing that production history and other dynamic data can be used to reconstruct the reservoir state. Fig. 10 shows that our methodology works well in 3-D. As in Fig. 10 even a crude discretization captures the overall reservoir shape.

6. Conclusions. We showed a self consistent method for most probable homogenized solution by integrating multiple scale analysis and information theory. The self consistency is in terms of level of upscaling in the reservoir simulator used and the spatial scale to which one would like to resolve the features of interest. Furthermore, the homogenization removes the great number of alternative solutions of the inverse problem which arise at scales less than that of the spatial resolution of data. The great potential of the method to delineate many fluid/rock properties across a reservoir is
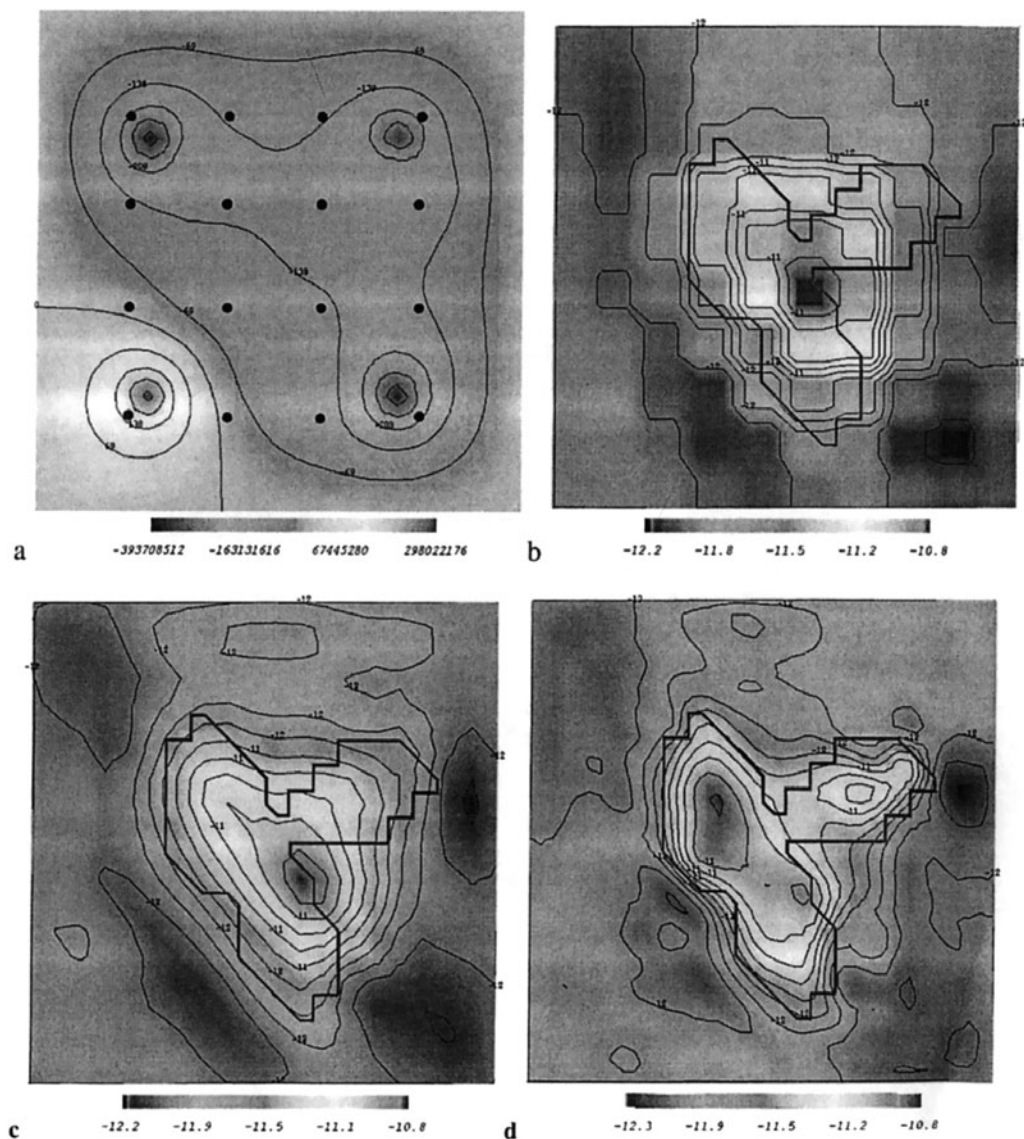
FIG. 7. (a) 2-D test domain (10 × 10 km) showing locations of 16 monitoring wells, and injection and production wells; color coded map of fluid pressure related to the configuration of injection/production wells and the nonuniform distribution of permeability. Our information technology was used to compute the assumed unknown permeability distribution. The calculation was made efficient by a multi-grid technique using 11 × 11 (b), 21 × 21 (c), and 41 × 41 (d) finite element resolution. The final result (d) is in good agreement with the actual high permeability zone indicated by the purple (outline across which the actual permeability jumps one order of magnitude).
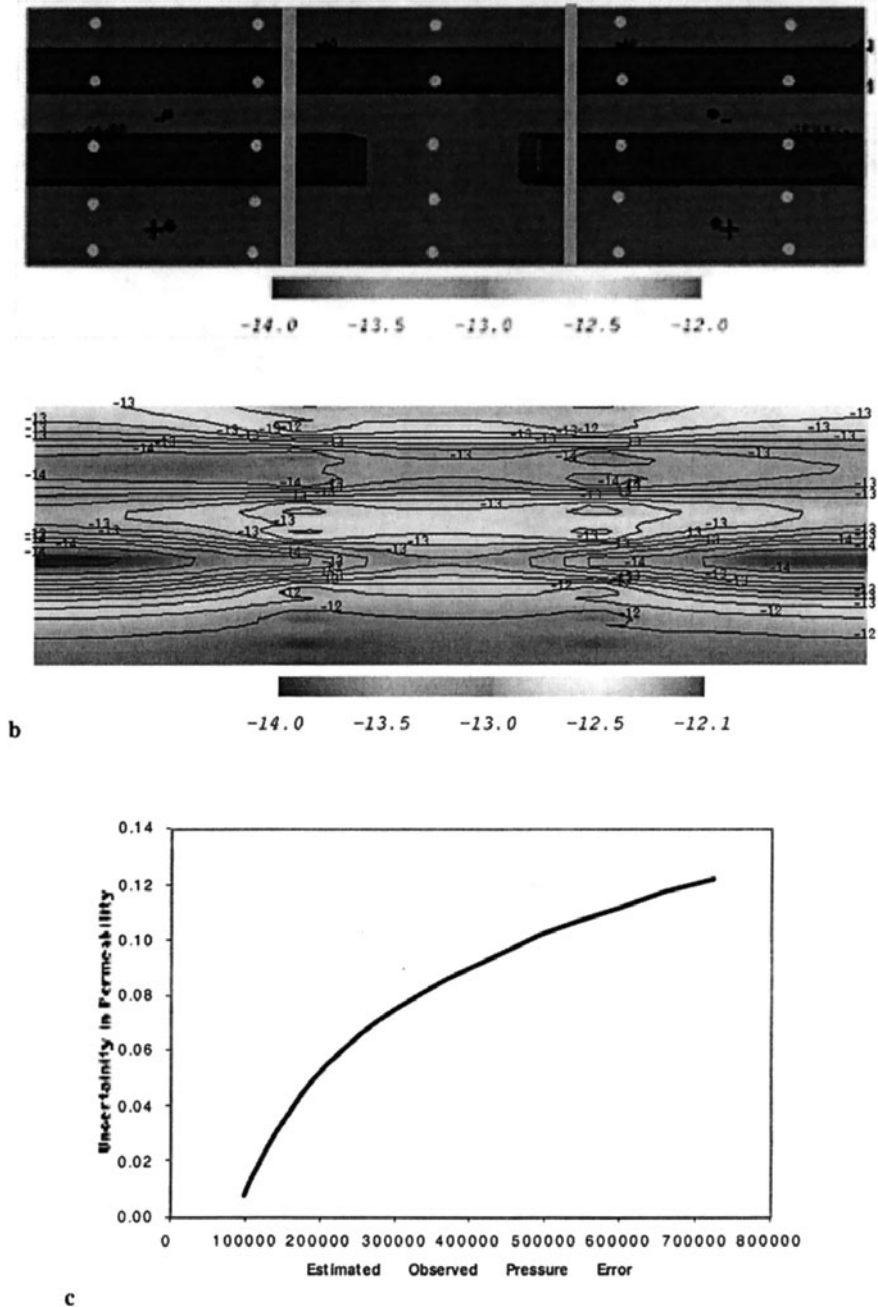
FIG. 8. *a) Cross-section view of an upper and lower reservoir separated by a seal with a puncture. Shown here is the actual permeability field, pressure monitoring well locations (yellow dots), production (−) /injection (+) well locations, and two permeability logs (vertical lines). The challenge is to predict the location and extent of the puncture that was missed by the two logs. b) We efficiently arrive at a prediction that captures the puncture even with limited production and core data. c) Uncertainty in the predicted permeability (as defined in equation (15)) as a function of estimated pressure monitoring/simulator error.*
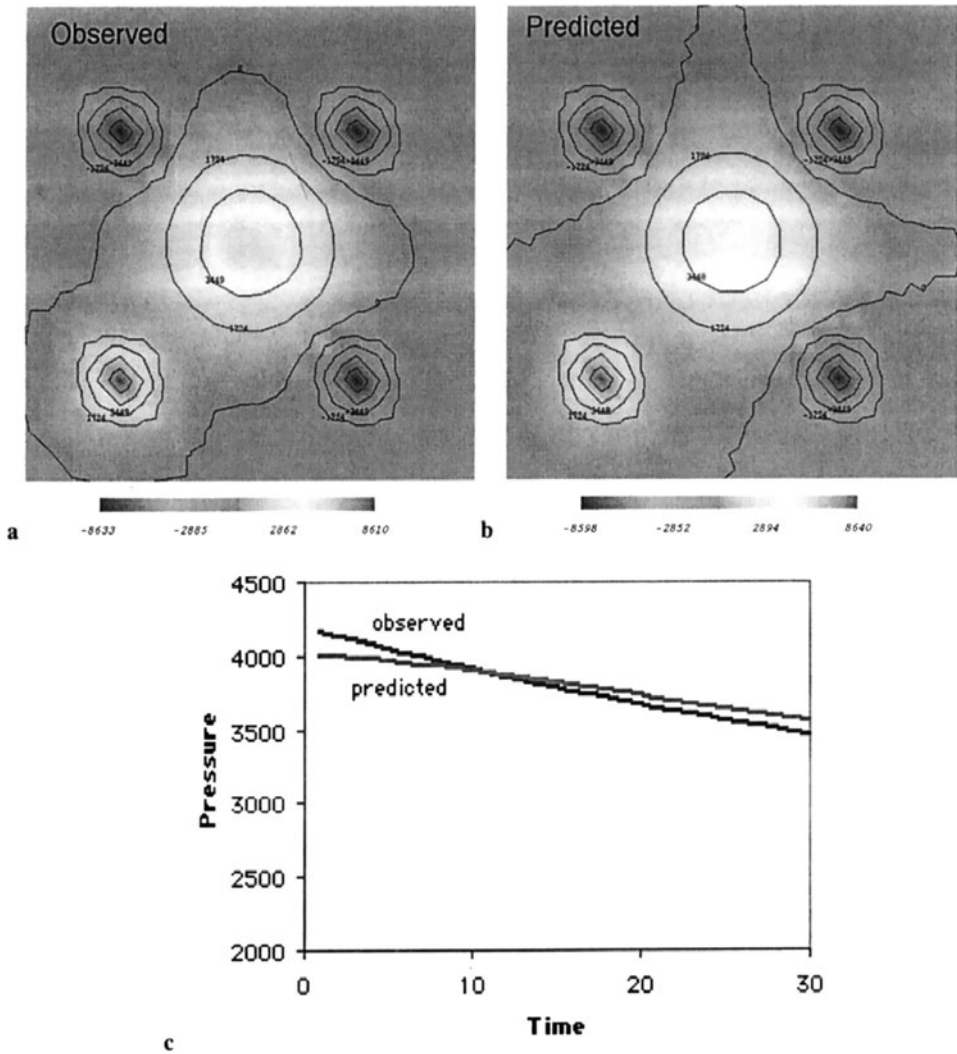
FIG. 9. *Predicted initial pressure distribution from (production history) information at selected wells. The approach here can also be used to predict the preproduction distribution of other reservoir state variables. a) Actual distribution of pressure after 30 days indicating locations of injection and production wells as pressure maxima and minima. b) Predicted distribution of pressure - note the excellent agreement with (a). c) Comparison of actual and predicted pressure at one of the pressure monitoring wells.*

only attained through the use of multiple RTM process simulators. We believe that our method is a major advance over presently used history matching algorithms due to self consistent treatment of multiple scales and direct approach to obtaining the most probable reservoir state. Finally having embedded the computations in an overall context of information theory, our approach yields a practical method for assessing risk.
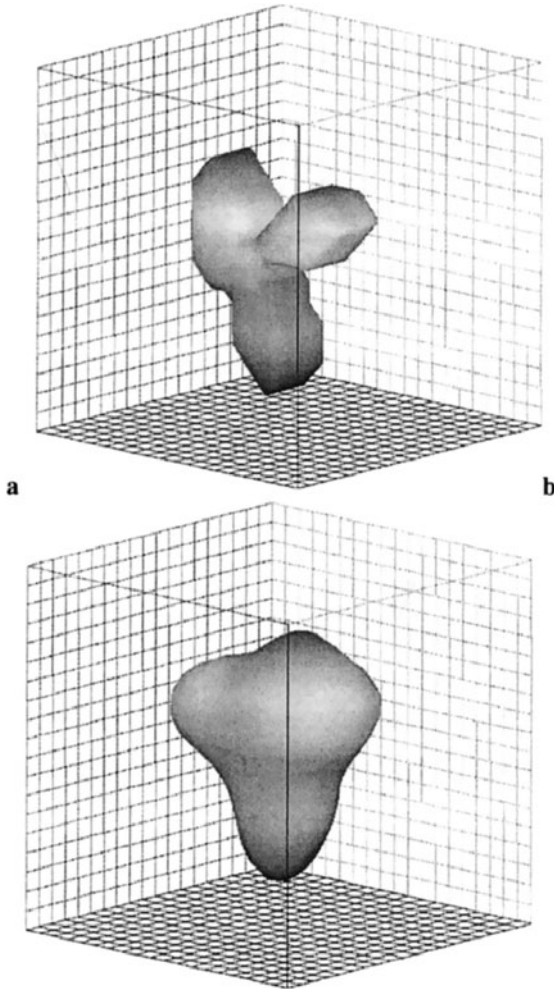
FIG. 10. *Our new iterative method works well in 3-D. Even a crude discretization can capture overall reservoir shape and location. Shown is a) the actual high permeability zone and b) that predicted by our approach for a 21 × 21 × 21 grid. The domain is 10 × 10 × 10 km. Smaller scale features in the actual permeability surface are lost on the predicted one because of the spacing of the pressure monitoring wells and the configuration of the production/injection wells, as we would expect.*

REFERENCES

GOMEZ-HERNANDEZ, J.J., A. SAHUQUILLO, AND J. CAPPILLA. 1998. Review of current approaches to integrate flow production data in geological modeling. *Journal of Hydrology* 203: (1–4), 162–174.

HU, L.Y., G. BLANC, AND B. NOETINGER. 1999. Gradual deformation of continous geostatistical models for history matching. *Proceeding of IAMG '99*, Trondheim, Norway.

HU, L.Y. 1999. Gradual deformation and iterative calibration of gaussian-related stochastic models. *Mathetical. Geology* 32: 87–108.

ORTOLEVA, P., E. MERINO, J. CHADAM, AND C.H. MOORE. 1987a. Geochemical self-organization I: Reaction-transport feedback mechanisms and modeling approach. American Journal of Science 287: 979–1007.

ORTOLEVA, P., E. MERINO, C.H. MOORE, AND J. CHADAM. 1987b. Geochemical self-organization II: The reactive-infiltration instability. American Journal of Science 287: 1008–1040.

ORTOLEVA, P., ed. 1990. Self-organization in geological systems: Proceedings of a Workshop held 26–30 June 1988, University of California at Santa Barbara. Earth-Science Reviews 29 (1–4) (special issue).

ORTOLEVA, P. 1992. *Nonlinear Chemical Waves*. Chichester: Wiley and Sons.

ORTOLEVA, P. 1994a. *Geochemical Self-Organization*. NY: Oxford University Press.

ORTOLEVA, P., ed. 1994b. *Basin Compartments and Seals*. AAPG Mem 61. Tulsa, OK: AAPG.

ORTOLEVA, P. 1998. *Basin compartment fundamentals*, Topical Report (No. GRI-97/0097). Chicago: Gas Research Institute.

ORTOLEVA, P., M. MAXWELL, D. PAYNE, AND W. SIBO. 1997. Naturally fractured reservoirs and compartments: A predictive basin modeling approach. In *Fractured reservoirs: Characterization and modeling*, RMAG 1997 Guidebook, edited by Thomas E. Hoak, Alan L. Klawitter, and Peter K. Blomquist, 227–242. Denver: Rocky Mountain Association of Geologists.

OZKAN, G. AND P. ORTOLEVA. 2000. Evolution of gouge grain size distribution: A markov model. *Pure and Applied Geophysics* 157: 10510–10525.

PAYNE, D., K. TUNCAY, A. PARK, J. COMER, AND P. ORTOLEVA. 2000. A reaction-transport-mechanical approach to modeling the interrelationships among gas generation, overpressuring, and fracturing: Implications for the Upper Cretaceous natural gas reservoirs of the Piceance basin, Colorado *AAPG Bull.* 84: 545–565.

RICE, J.R. 1975. Continuum mechanics and thermodynamics of plasticity in relation to microscale deformation mechanisms. In *Constitutive Equations in Plasticity*, edited by A. S. Argon, 23–79. Cambridge, Mass.: MIT Press.

ROGGERO, F. AND L.Y. HU. 1998. paper SPE 49004, Gradual deformation of continous geostatistical models for history matching. presented *at 1998 SPE Annual Technical Conference and Exhibition,*New Orleans, LA, September 27–30.

TRAN, T.T., X.H. WEN, AND R.A. BEHRENS. 1999. Efficient conditioning of 3D fine-scale reservoir model to multiphase production data using streamline-based coarse-scale inversion and geostatistical downscaling. Paper SPE 4897, presented *at 1999 SPE Annual Technical Conference and Exhibition,* Houston, TX Oct. 3–6.

TUNCAY, K., A. PARK, AND ORTOLEVA, P. 2000a. Sedimentary basin deformation. *Tectonophysiscs* 323: 77–104.

TUNCAY, K., A. PARK, AND P. ORTOLEVA. 2000b. A forward fracture model to predict fracture orientation and properties. *J. Geophys. Res.* 105: 16719–16735.

TUNCAY, K., A. KHALIL, AND P. ORTOLEVA. 2001. Failure, memory and cyclic fault movement. *Bulletin of Seismological Society of America* 91: 538–552.

TUNCAY, K. AND P. ORTOLEVA. 2001. Salt tectonics as a self-organizing process. *J. Geophys. Res.* 106: 803–818.

WEN, X.H., C.V. DEUTSCH, AND A.S. CULLICK. 1998a. *Geostatistical Software Library and User's Guide,* 2nd edition, Oxford University Press.

WEN, X.H., C.V. DEUTSCH, AND A.S. CULLICK. 1998b. paper SPE 48971, presented *at 1998 SPE Annual Technical Conference and Exhibition,*New Orleans, LA, September 27–30.

WEN, X.H., J.E. CAPILLA, J.E., DEUTSCH, C.V. GOMEZ-HERNANDEZ, AND A.S. CULLICK. 1999. *Computers and Geosciences,* 25: 217–230.

WEN, X.H., T.T. TRAN, R.A. BEHRENS, AND J.J. GOMEZ-HERNANDEZ. 2000. *SPE International* 6303: 1–13.

ZIENKIEWICZ, O.C., AND I.C. CORMEAU. 1974. Visco-plasticity and creep in elastic solids - A unified numerical solution approach. *Int. J. Num. Met. Eng.* 8: 821–845.